

Research Article www.acsami.org

Ion Dynamics of Monomeric Ionic Liquids Polymerized In Situ within Silica Nanopores

Thomas Kinsey, Kaitlin Glynn, Tyler Cosby, Ciprian Iacob, and Joshua Sangoro*



Cite This: ACS Appl. Mater. Interfaces 2020, 12, 44325-44334



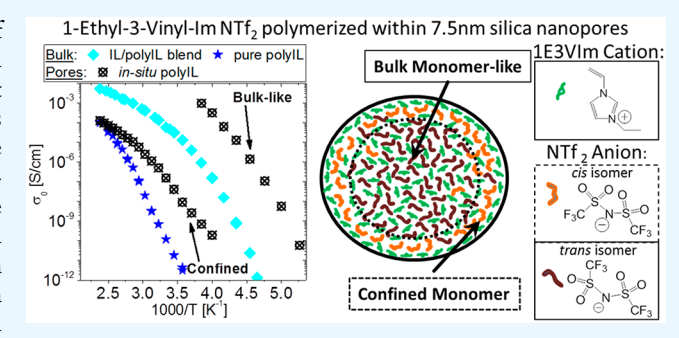
ACCESS I

Metrics & More

Article Recommendations

Supporting Information

ABSTRACT: Polymerized ionic liquids are a promising class of versatile solid-state electrolytes for applications ranging from electrochemical energy storage to flexible smart materials that remain limited by their relatively low ionic conductivities compared to conventional electrolytes. Here, we show that the in situ polymerization of the vinyl cationic monomer, 1-ethyl-3vinylimidazolium with the bis(trifluoromethanesulfonyl)imide counteranion, under nanoconfinement within 7.5 ± 1.0 nm diameter nanopores results in a nearly 1000-fold enhancement in the ionic conductivity compared to the material polymerized in bulk. Using insights from broadband dielectric and Raman spectroscopic techniques, we attribute these results to the role of



confinement on molecular conformations, ion coordination, and subsequently the ionic conductivity in the polymerized ionic liquid. These results contribute to the understanding of the dynamics of nanoconfined molecules and show that in situ polymerization under nanoscale geometric confinement is a promising path toward enhancing ion conductivity in polymer electrolytes.

KEYWORDS: polymerized ionic liquids, nanoconfinement, ion dynamics, molecular conformations, Raman spectroscopy, broadband dielectric spectroscopy

■ INTRODUCTION

By combination of the robust mechanical properties of polymers with the ion conduction capabilities and electrochemical stability of room temperature ionic liquids (ILs), polymerized ionic liquids (polyILs) have emerged as a promising class of highly tunable materials for a wide range of applications including battery technologies, fuel cell membranes, CO2 capture, biomolecule detection, nanoactuators, and stimuli-responsive materials. 1-4 The fast ion diffusion compared to the time scale of the structural dynamics of the polymer segments is the main distinguishing characteristic of these materials compared to typical solid polymer electrolyte systems. However, the effective immobilization of one of the ions onto the polymer backbone following polymerization drastically reduces the overall ionic conductivity compared to the unpolymerized ILs. Other changes in physicochemical properties that result from polymerization include a decrease in molecular degrees of freedom and increased viscosity, both of which affect ion mobilities.^{6,7} There have been several attempts to increase ionic conductivity in ILs through various chemical and physical methods, one of which is the use of physical confinement at nanometer length scales.⁸⁻¹¹ However, the effects of physical confinement at the molecular level on the properties of polyILs and the question of whether it is possible to achieve high ionic

conductivity through geometric nanoscale confinement remain unexplored.

Geometric confinement at the molecular level is known to result in significant changes in the physical properties of various glass-forming systems by altering the length scales of cooperative dynamics and/or increasing the role of substrate interactions. ^{12–16} Additionally, the behavior of ions in nanopores is of great importance for engineering nanofluidic and biosensing devices, and the mechanism of ion transport through nanochannels is of much interest for biomimetic technology such as cellular transistors and selective filtration. 17-21 For pure ILs under nanoconfinement, reports have identified that influences from both the length scale of the confinement and the electrostatic surface interactions of the ions with the substrate can either facilitate or hinder ion transport.²²⁻²⁵ Experimental and simulation studies of ILs have suggested that there is an increase in the coordination between the anion and cation near the substrate which can result in slowed ion diffusion compared to the bulk. 9,26

Received: July 8, 2020 Accepted: September 4, 2020 Published: September 4, 2020





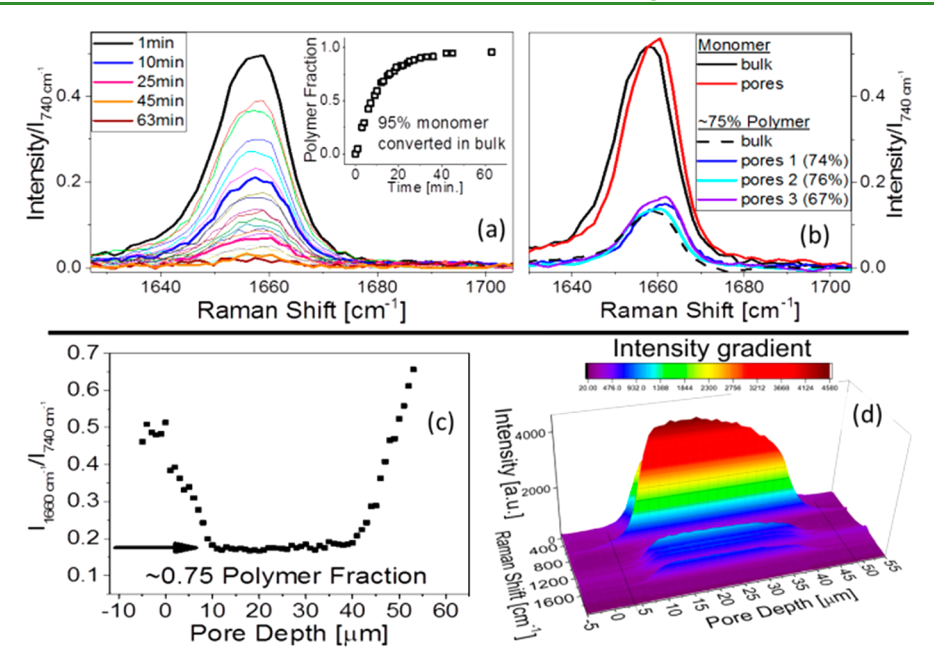


Figure 1. Normalized Raman spectra showing decreasing intensity of the 1660 cm^{-1} band over time during bulk polymerization (a) as well as before and after *in situ* polymerization and bulk 75% polyIL/IL blend (b). The inset of (a) shows that the calculated polymer fraction during bulk polymerization over time with a final monomer conversion of 95%. Confocal Raman Z-mapping normalized by I_{740} after polymerization within pores (c) and non-normalized 3D data plot (d) reveals that the pores are uniformly filled with IL and polyIL.

Furthermore, ordered solvation layers of up to several ion pairs, which also correspond to a reduction in ion mobility, have been shown to occur under confinement and near the substrate interface due to these electrostatic surface interactions of the ILs and the substrate. 27-30 On the other hand, faster dynamics in nanoporous media have also been observed as the confinement length scale increases and the strength of interactions with the substrate decreases. 31,32 These faster dynamics with increasing confinement have been utilized to help design synthetic biomimetic ion channels and polymerbased nanofluidic diodes. 19,33,34 Finally, the conformational equilibrium structures of the IL moieties have been observed to change under confinement, which may also alter dynamics. 35,36 Therefore, nanoscale confinement seems to be a promising approach to tune physicochemical properties of polyILs.

For noncharged polymers under nanoconfinement, several physical characteristics have also been observed to change compared to bulk including the dynamic glass transition temperature (T_g) , self-diffusivity, dielectric relaxation strength, conformational entropy, and molecular packing density. 16,37 Similarly, these structural and dynamical effects that are observed under nanoconfinement have also been observed in pressure-dependent studies of noncharged polymer systems. 14,42-46 Additionally, in situ free radical polymerization within anodized aluminum oxide (AAO) nanopores have resulted in an increase in reaction kinetics with the resulting polymers exhibiting a narrower molecular weight distribution compared to those prepared under similar reaction conditions in bulk. 47,48 For bulk polyILs, experimental and computational studies have shown that when the ion conduction is dominated by hopping of ions along the polymer backbone corresponding to faster dynamics compared to hopping from chain to chain in an entangled system. 46,49,50 Thus, if nanoscale confinement can lead to favorable alignment of chains as seen in noncharged polymers, then higher ionic conductivity may result in polyILs.

However, very few studies have examined the effects of surface interactions and confinement on the properties of poly-ILs. 48,49,51

To unravel the interplay between confinement on the molecular conformations and ionic dynamics of nanoconfined polyILs, the well-studied monomeric vinyl IL, 1-ethyl-3vinylimidazolium [1E3VIm] with the bis(trifluoromethanesulfonyl)imide [NTf₂] counteranion, was filled into unidirectional nanoporous silica membranes with mean pore diameter of 7.5 nm and subsequently polymerized in situ by free radical polymerization. Broadband dielectric spectroscopy (BDS) and Raman spectroscopy were employed to study the changes in the dynamics and ion conformations and coordination that result from both the nanoconfinement and polymerization. The ionic conductivity of the confined polyIL was observed to increase by a factor of \sim 1000 compared to the bulk equivalent. We attribute the enhancement in charge transport of the confined polyIL to changes in the equilibrium ratio of the NTf₂ cis and trans conformational isomers and decreased coordination between cations and anions. We demonstrate that these changes arise from (i) screened electrostatic interactions of the substrate with the free anions, (ii) lower packing density of the polyIL within the pores, and (iii) implicit unidirectional alignment of polymer chains within the nanopores that result in increased mobility of the NTf2 anion.

■ RESULTS AND DISCUSSION

Prior to investigating the properties of the nanoconfined polyIL, it is critical to have a measure of the degree of polymerization, fraction of unreacted monomer, and extent of nanopore filling. These factors are readily probed by confocal Raman spectroscopy and complementary ¹H NMR measurements. First, the progression of free radical polymerization in bulk and nanoconfined 1E3VIm NTf2 is investigated. Prior to further analysis, all Raman spectra were baseline corrected and normalized by the integrated intensity of the S–N–S bending

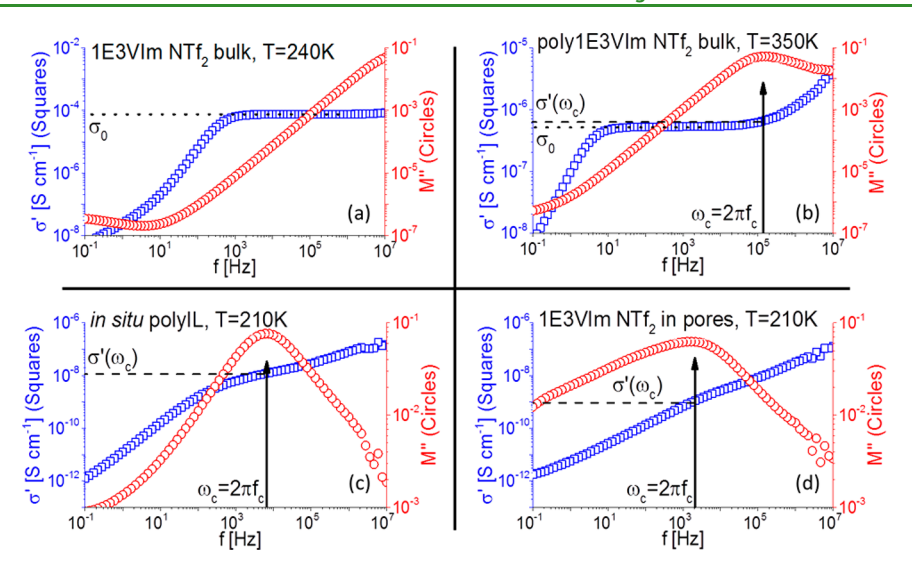


Figure 2. Frequency-dependent real part of the complex conductivity (σ' , left axis) and imaginary part of the electric modulus (M'', right axis) versus frequency for bulk monomer at 240 K (a), bulk polymer at 350 K (b), in situ polyIL at 210 K (c), and 1E3VIm NTf₂ at 210 K (d). The frequency of the peak maximum in M'' is indicated with vertical arrows at f_c . The horizontal dotted lines indicate the value of σ_0 for the bulk monomer and polymer samples. The dashed lines signify the σ' values at the frequency of the main M'' peak which corresponds to the onset of long-range ion hopping.

mode of the NTf₂ anion, I_{740} , to account for changes in the density of the material during polymerization. The C=C stretching mode of the vinyl group on the cation shows up as a band at 1660 cm⁻¹ in the Raman spectrum. As shown in Figure 1a, this peak reduces in strength as polymerization proceeds due to reaction of the vinyl bond into the polyIL backbone. The percent conversion of the monomeric cations into polymeric repeat units within the chain backbone was calculated over time (i.e., polymer fraction = $[I_{t=0} - I_t]/I_{t=0}$, where I_t is the integrated intensity of the normalized 1660 cm⁻¹ peak at initial time, t=0, and as time progressed during polymerization). These polymer fraction data are displayed in the inset of Figure 1a and reveal a final monomer percent conversion in bulk of ~95%. The resulting polymer was measured by H NMR to determine the number-average molecular weight of $M_n = 5.2$ kg/mol.

Using the data in the inset of Figure 1a as a calibration basis for polymer fraction, we determined the percent conversion of monomeric cations into polymer repeat units under nanoconfinement to be $72 \pm 4\%$ over three separate experiments (see Figure 1b). A Z-mapping spectrum of the polymerized 1E3VIm NTf₂ in the nanopores, with an accuracy of ± 50 nm, was obtained by using confocal Raman microscopy and is displayed in Figure 1d. The depth profile of the normalized I_{1660} in Figure 1c reveals that the resulting polymer and unreacted monomer are uniformly filled through the pores after polymerization. Assuming no termination by combination, the $M_{\rm n}$ of resulting polymer was estimated to be ~3 kg/ mol by ¹H NMR from the data in Figure S1. For comparison, a bulk blend of a $M_n = 3.2 \text{ kg/mol polyIL}$ was prepared with 75 mol % monomer as described in the Materials and Methods section. Figure 1b shows that the intensity of the 1660 cm⁻¹ peak for the bulk 75% polymer/monomer blend is comparable to that of the confined polymer sample. This bulk mixture and neat polyIL will be henceforth termed the "75% polyIL/IL blend" and "bulk polyIL", respectively, and the nanoconfined IL and polymerized samples will be termed the "1E3VIm NTf_2 in pores" and "in-situ polyIL", respectively. We note that because of the low emission intensity of the ILs in nanopores

and instrument limitations during temperature control measurements, Raman measurements were not successful during the *in situ* polymerization within pores (see the Materials and Methods section for details). Therefore, only measurements made before and after polymerization are reported here.

From the BDS experiments, the real part of the complex conductivity (σ') and imaginary part of electric modulus (M'')are plotted against frequency in Figure 2 for all samples except for the bulk 75% polyIL/IL blend. The dielectric spectra of bulk materials result in qualitatively similar data with a characteristic frequency-independent plateau corresponding to the DC ionic conductivity (σ_0). The polymer and monomer confined within the nanopores, however, do not display a characteristic plateau for σ_0 . The most probable reasons for this are a distribution in pore sizes and mobility deviations at such small length scales that cause an increased distribution of polarization time scales. ^{32,48} Therefore, the M" peak frequency (ω_c) is taken to denote the characteristic rate of the onset of long-range ion hopping, and the value of σ' at ω_c is used to estimate σ_0 for all samples except the bulk monomeric IL. The $\sigma'(\omega_c)$ values are typically higher than σ_0 by a factor of about 2 (see Figure 2b) but are often used when the distribution of ion hopping relaxations is not clearly represented by a single onset

Below 240 K, the monomer in bulk crystallizes and σ_0 drops considerably, and the time scales of ω_c occur outside the accessible frequency range. Therefore, the actual σ' plateau value, σ_0 , is taken as the σ_0 for this sample. Crystallization does not occur for any of the other samples in bulk or in pores, and therefore, the $\sigma'(\omega_c)$ values are used as an estimation of σ_0 for relative consistency. In Figure 3, M'' and normalized σ'/σ_0 data from 190 to 230 K are plotted together as master curves by normalizing the angular frequency by ω_c for the *in situ* polyIL and 1E3VIm NTf₂ in pores. This representation of M'' shows that the breadth of the main peak is narrower for the *in situ* prepared polyIL compared to the 1E3VIm NTf₂ in the nanopores. This suggests a more homogeneous distribution of ion dynamics time scales for the *in situ* polyIL samples. In the

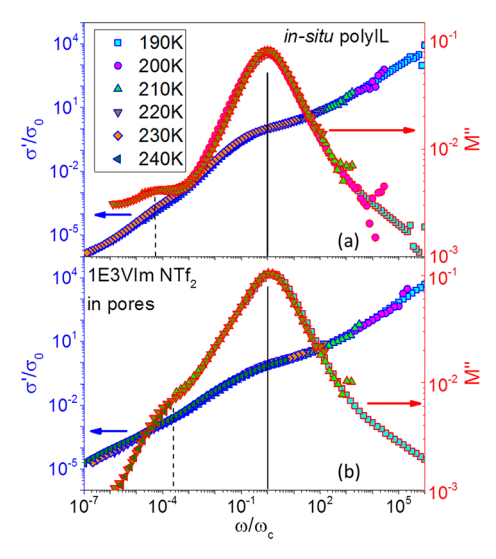


Figure 3. Master curves of the real part of the complex conductivity (σ') and the imaginary part of the electric modulus (M'') functions versus the radial frequency scaled by the characteristic ion transport rate (ω_c) for confined polymer (a) and monomer (b). The real part of conductivity (blue edged data) is normalized by the ionic conductivity, σ_0 (left axis). These master curves were prepared by normalizing the frequency-dependent spectra at each temperature by ω_c . Vertical lines are added as guides to the eye, denoting the main peak at ω_c and the lower frequency peak of confined polymer and monomer ion dynamics, respectively.

Figure 3 M'' master curves, another lower-frequency, higher-temperature peak is present with a weaker intensity than the $M''(\omega_c)$ relaxation for both the 1E3VIm NTf₂ in pores and in situ polyIL. This relaxation is slightly perceptible as a low-frequency shoulder in the single-temperature spectra of Figure 2c. This slower relaxation is ascribed to interfacial ion dynamics that are not observed in bulk, presumably arising from electrostatic interactions at the substrate interface. ²⁶

The representative ionic conductivities are plotted versus inverse temperature for all materials in Figure 4, along with the σ' values associated with the lower-frequency M'' peak for the nanoconfined samples which are labeled with "confined polymer" and "confined monomer". The values for the *in situ* polyIL and 1E3VIm NTf₂ in pores in Figure 4 are corrected for

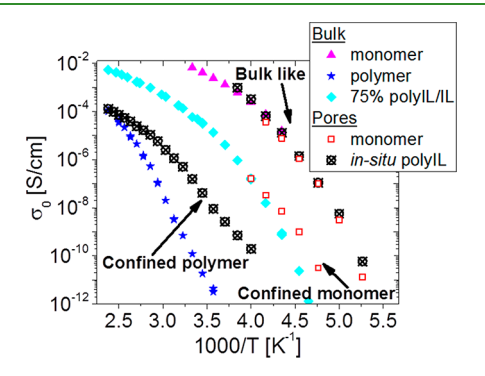


Figure 4. The dc ionic conductivity $(\sigma_0 \sim \sigma'(\omega_c))$ plotted against inverse temperature for all ILs and polyILs (see legend). For nanoconfined samples, the main $\sigma'(\omega_c)$ values are signified with the arrow denoting "bulk-like" conductivities. The data labeled "confined polymer" and "confined monomer" are the σ' values that correspond to the lower-frequency, higher-temperature M'' peak shown in Figure 3.

the 7% porosity of the silica membranes. The linear relation in the log–log plot of σ_0 and ω_c (termed the Barton–Nakajima–Namikawa relation, BNN) holds for all samples as seen in Figure S2. As expected, the 75% polyIL/IL blend has a lower conductivity compared to the bulk IL with a similar Vogel–Fulcher–Tammann (VFT) temperature dependence, whereas the bulk polyIL displays an Arrhenius-like temperature dependence especially at low temperatures. This suggests that at this concentration for the 75% polyIL/IL blend the chain packing frustration may not be significant enough to have decoupled ionic conductivity from ion dynamics as observed in bulk for neat imidazolium-based polyILs. $^{\rm S,7}$ However, this consideration is beyond the scope of the current article.

The ionic conductivity of the 1E3VIm NTf2 in pores is similar to that in bulk and is consistent with past reports. 31,32,48 The "confined polymer" conductivity of the in situ polyIL in Figure 4 is observed to be similar to the polyIL in bulk at high temperatures. However, since the "confined polymer" conductivity exhibits a decreased activation energy, the resulting ionic conductivity at room temperature is 3 decades greater than that of bulk polyIL. We attribute this result mainly to alignment of polymer chains through the pore allowing for the single chain ion hopping mechanism which has been estimated by simulations to contribute to enhancement of ion transport compared to intrachain hopping. 56 Through transport flux considerations, an equation for dc conductivity (σ_0) can be formulated as a linear combination of the products of mobility (μ) , number density (n), and charge (q) of all the ions (i) in the system: $\sigma_0 = \sum_i \mu_i n_i q_i$. Following polymerization, it is reasonable to expect that the effective number density of charge carriers (n) would not differ by orders of magnitude. By assuming no effective change in the charge of each ion, the main contribution to increase the dc conductivity toward lower temperatures for the polyIL in the pores therefore must be the mobility of the ions (μ) . Additionally, the fact that there is an obvious bifurcation in the time scales of ion dynamics for the in situ polyIL, which is not observed in the similar bulk material of the 75% polyIL/IL blend, strongly suggests heterogeneous dynamics of the polymerized 1E3VIm NTf₂ material within the silica pores. These heterogeneous dynamics will be explored further in the discussions on ion conformation and coordination below.

To investigate the roles of confinement and polymerization on the NTf2 conformations and anion-cation coordination, we will now return to the Raman data. The NTf2 anion is known to take on both cis and trans conformational isomers, which in the literature are called the C1 and C2 conformers, respectively. 35,57-59 In Figure 5a, the room temperature Raman peaks at 398 and 410 cm⁻¹ that correspond to the C2 and C1 conformers, respectively, are displayed for all of the samples in this study. The relative integrated intensities of these peaks (I_{398} and I_{410}) correspond to the conformational equilibrium concentrations of the NTf₂ trans and cis isomers.⁶⁰ The monomer samples, in both bulk and nanoconfinement, have a relatively decreased I_{410} , indicating that the monomer samples have a significantly decreased fraction of the C1 conformer, whereas the bulk polyIL and 75% polyIL/IL blend samples have an increased equilibrium concentration of this cis isomer. Interestingly, the in situ polyIL is found to have a similarly low fraction of the C1 conformer as both of the monomer samples. In Figure 5c, the cis and trans isomer peaks at selected times measured during bulk polymerization at 85

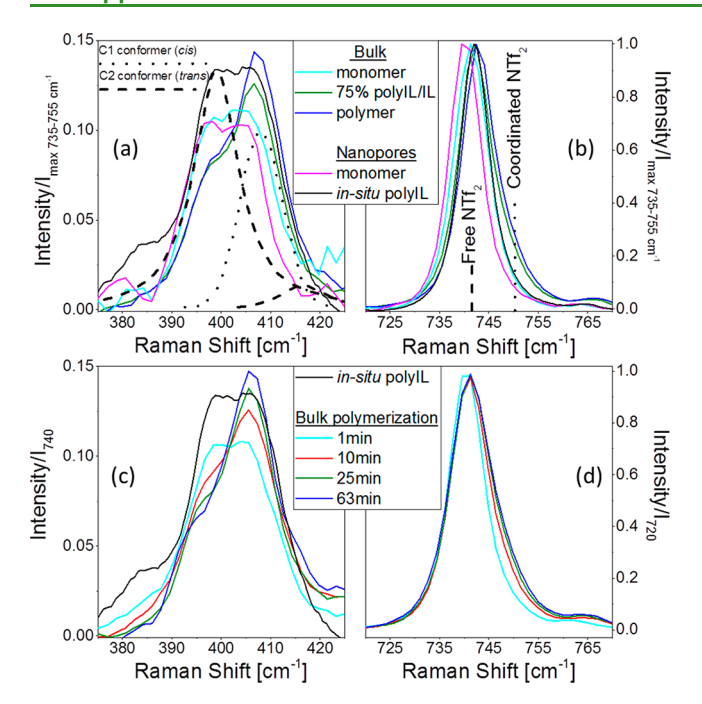


Figure 5. Raman spectra associated with the NTf₂ *cis* (dotted) and *trans* (dashed) conformations at 410 and 398 cm⁻¹, respectively, for bulk samples, monomer in pores, and *in situ* polyIL (a) and during bulk polymerization measurements (c). The S-N-S bending mode observed at \sim 740 cm⁻¹ is displayed for all materials (b) and during bulk polymerization measurements (d). In (b) the dashed and dotted lines signify bands corresponding to free anions and more coordinated anions, respectively. All are normalized by peak intensity of the S-N-S bending mode at \sim 740 cm⁻¹ to account for density variations among the samples.

°C show that the relative amount of NTf₂ conformations shifts to a higher concentration of *cis* isomers as polymerization progresses. This shift occurs at ~10 min following initiation and corresponds to a polymer fraction of about 0.7. Correspondingly, the 75% polyIL/IL blend at room temperature has a similar I_{398} to I_{410} ratio as the bulk polymerization at 85 °C during Raman measurement at 10 min. Therefore, we conclude that the increased equilibrium concentration of the C1 conformer in the bulk 75% polyIL/IL blend compared to an increased C2 conformer concentration for the *in situ* polyIL is a direct result of confinement of the material within the 7.5 nm diameter nanopores.

The equilibrium conformational changes of the NTf2 anion are well documented in the literature for ILs and metal ion salts. Higher equilibrium concentrations of the C2 conformer in NTf2 containing ILs have been observed in crystalline domains and at higher pressures, while the C1 conformer has been calculated to have reduced conformational entropy and larger dipole moments. 61,62 Additionally, it has been determined that packing density and conformation play a crucial role in crystallization and glass formation of NTf2 containing ILs. 43 Therefore, these NTf2 isomers can be used as a proxy for considering possible changes in the molecular density of the materials in this study. Furthermore, recent results of polymers confined to silica nanopores showed that for poly(propylene glycol) a density gradient of chain forms where lower densities occur at the center of the pore.¹⁶ The same group also reported evidence of density fluctuations that determine the glassy dynamics of alcohols in nanopores from positron lifetime annihilation spectroscopy and BDS measurements. 12 Considering our results in combination with conformational and density changes reported in the literature, we conjecture that a higher NTf₂ equilibrium concentration of the C1 conformer in our materials can be qualitatively used as a proxy for determining which materials have a comparatively higher packing density. As such, the *in situ* polyIL sample has a lower average packing density than the bulk samples that contain polyIL. This lower density within nanoconfinement then corresponds to a relatively higher concentration of C2 conformers, which also corresponds to materials with the highest ionic conductivities (e.g., monomeric IL and nanoconfined materials).

An additional feature of the Raman spectra of ILs containing the NTf₂ anion is the \sim 740 cm⁻¹ band corresponding to S-N-S bending modes. A blue-shift in this \sim 740 cm⁻¹ band (i.e., shift toward lower wavenumbers) has been determined to correspond to NTf2 ions that are less coordinated with the countercation. 52,60 Density functional theory calculations show that this peak is actually a combination of two peaks: one that increases in intensity at 748 cm⁻¹ corresponding to NTf₂ ions that are more coordinated to the cation and one that conversely increases in intensity at $742~\text{cm}^{-1}$ as the anion becomes less coordinated. We performed temperaturedependent bulk measurements of the bulk IL and polyIL, corroborating this effect through observation of a blue-shift of the peak with decreasing temperature (see Figure S3). The narrower width in the $M''(\omega_c)$ peak, which is observed following polymerization in nanopores in Figure 3, has been shown to also correlate with increased average ion-to-ion distances in salts.⁶⁴ The following qualitatively lists the materials in this study in increasing shift toward more coordinated anions in Figure 5b: 1E3VIm NTf2 in pores > bulk 1E3VIm NTf₂ > in situ polyIL > bulk 75% polyIL/IL blend > bulk poly1E3VIm NTf₂. Figure 5d shows the ~740 cm⁻¹ peak during bulk polymerization over time. Here, the peak maximum does not actually shift, but a more pronounced shoulder at 748 cm⁻¹ is observed. Overall, the results in Figure 5 show that the less coordinated NTf2 having a higher degree of C1 conformers is favored under confinement.

We now analyze the ionic conductivity data of the ILs from Figure 4 to determine the fraction of ions that are adsorbed at the silica substrate and make a decreased contribution to longrange ion motion. Because of the parallel geometry of the porous silica matrix and the material in the pores, complex impedance (Z^*) can be separated into a linear combination of contributions from the SiO_2 matrix $(Z_{SiO_2}^*)$ and the material inside the pores (Z_{pore}^*) . The complex impedance is related to the measured complex dielectric function (ε_m^*) through Z^{*-1} = $i\omega \varepsilon_m^* C_m$, where C_m is the vacuum capacitance associated with the sample geometry and $\varepsilon_{\rm m}^*$ is the complex dielectric function. Here, for $\varepsilon_{\rm m}^* = \varepsilon_{\rm m}' - i\varepsilon_{\rm m}''$, $\varepsilon_{\rm m}''$ and $\varepsilon_{\rm m}''$ are the measured real and imaginary parts of the complex dielectric function, respectively. In reports by Iacob et al., the authors used a linear combination of the measured imaginary permittivity to describe dynamics of nanoconfined ILs based on surface area fractions of adsorbed and nonadsorbed ions. 32,65 We will use a slightly different representation using the real part of the measured complex conductivity, $\sigma_{\rm m}' = \omega \varepsilon_0 \varepsilon_{\rm m}''$, to express the dc conductivity values $(\sigma_{\rm m}'(\omega_{\rm c}))$ of the 1E3VIm NTf $_2$ in pores in terms of the contributions from the silica (σ'_{SiO_2}) and contributions from the materials in the pores separated into some layer adsorbed to the pore surface (σ_a) and some

contribution that is bulk-like toward the center of the pore (σ'_b) . This is displayed in eq 1, where the fractions parallel to electrodes for the adsorbed, bulk-like, and silica matrix are given by f_a , f_b , and $f_{SiO,}$, respectively.

$$\sigma_{\rm m}' = \sigma_{\rm d}'_{\rm a} + \sigma_{\rm b}'_{\rm b} + \sigma_{\rm SiO}' f_{\rm SiO}, \tag{1}$$

Even with a porosity of ~7% ($f_b + f_a = 0.07$ and therefore f_{SiO_2} ~ 0.93), the ion conducting properties of the SiO₂ matrix are so small at measured temperatures and frequencies ($\sigma'_{SiO_2} + f_{SiO_2} < 10^{-8} \text{ S cm}^{-1}$) that the σ'_{SiO_2} term in eq 1 is negligible compared to that of the ions within the pores. Dividing the terms in eq 1 by the bulk conductivity, $\sigma'_b(\omega_c)$, gives us a ratio of the measured conductivity to the conductivity of the bulk fraction ($\sigma'_m/\sigma'_b = f_b$, assuming $\sigma'_a \ll \sigma'_b$). From this we can calculate an estimated fraction of ions that are adsorbed to the pore wall and are inhibited from contributing to the dc conductivity ($F_a = f_a/0.07$). This fraction of adsorbed ions is displayed in Figure 6, where $F_a \sim 0.55$ ($f_a \sim 0.038$) is constant

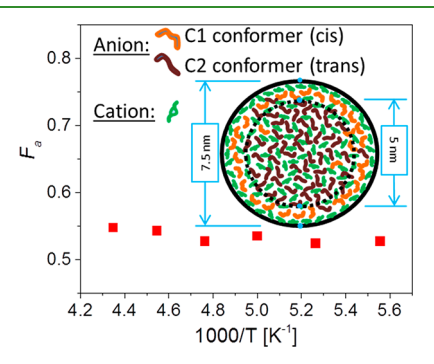


Figure 6. Illustration of the emerging picture of the fraction of ions that are adsorbed to the pore walls (F_a) vs inverse temperature. The inset schematic is a representation of the cross section of a silica nanopore filled with the 1E3VIm NTf₂ monomer. The pore walls are closely associated with cationic monomers which are then surrounded by a layer of anions with the *cis* conformation that exist within this F_a boundary as signified by concentric dotted circle with a 5 nm diameter. C2 conformers are present near the center of the pore and contribute to bulk like ion conduction as shown in Figure 2.

with temperature. Using this model, Iacob et al. found that from 220 to 250 K the absorbed surface area fraction of the entire silica membrane with 7.5 nm pores filled with 1-hexyl-3-methylimidazolium PF₆ increases from $f_{\rm a}\sim 0.04$ to 0.055, which agrees well with our simple estimation of adsorbed ion fractions.³²

With the ionic radii calculated for NTf_2 (\sim 1.85 Å) and 1-ethyl-3-methylimidazolium (\sim 1.5 Å) by Nordness et al., we have sketched a 7.5 nm diameter pore filled with 1E3VIm NTf_2 monomer, which is displayed roughly to scale as a schematic inset of Figure 6 with \sim 11 ion pairs spanning the diameter of the pore. The native OH bonds of SiO_2 are known to have a slightly negative charge and, therefore, preferentially interact with the cation. The schematic first displays an adsorbed layer of 1E3VIm cations near the pore surface (in green) closely coordinated with a second layer of anions having the C1 conformer (in orange) that correspond to a larger dipole moment of the NTf_2 anion. This picture is reinforced by results that show that imidazolium cations orient planar to silica surfaces, and the SO_2 oxygens of the NTf_2 anion in the cis conformation are closely coordinated to the imidazolium

ring. 52,66 From the calculated $F_{\rm av}$ a dotted concentric circle which has a radius of 2.5 nm and 0.45 surface area fraction of the 7.5 nm pore cross-sectional area is also displayed in the schematic. Within the pore, a count of the cations in the bulk-like layer inside the 5 nm diameter dotted circle constitutes \sim 70% of the cations packed inside the pore. This percentage of adsorbed ions closely resembles the fraction of monomers converted into the polymer backbone (*in situ* polyIL having 72 \pm 4% conversion of monomers; see Figure 1b). We expect that these cationic monomers that are effectively immobilized by the electrostatic solvation layer during polymerization remain largely unreacted.

The spatial resolution of the Raman microscope in the X-Yplane is limited to ~50 nm, and thus, we cannot experimentally determine changes in anion conformations across a single pore or whether the confined cations in the resulting polymer chains are more closely coordinated to the pore walls or the center of the pores or homogeneously distributed within the pore. However, it is evident from the confocal Z-mapping data in Figure 1c,d that the pores are uniformly filled with polyIL and IL, which suggests that the polymer chains take on a stretched conformation in the longitudinal direction. This is supported by results of noncharged polymers displaying nonequilibrium dynamics corresponding to stretched chain conformations. 41 Using this molecular picture and our results, we expect that the entropic penalty of polymerization in the nanopore is offset by the altered density of the in situ polyIL compared to the 75% polyIL/IL blend as suggested by the NTf2 conformational equilibrium data in Figure 5a. If we consider this penalty in bulk, the entropic cost may be offset by an increased fraction of the larger dipole moment C1 conformer following polymerization, which is similarly observed during crystallization. 43,62 Additionally, there is a reduced anion-cation coordination of the in situ polyIL compared to the polymer in bulk as shown for the blue-shift of the S-N-S bands in Figure 5b. Therefore, as polymerization progresses and reaches a maximum conversion under nanoconfinement, the resulting ion conduction associated with the polymer chains elongated through the pores is higher than the random coiled chains of the bulk polymer as shown in the "confined polymer" conductivity in Figure 3. Additionally, the ion hopping mechanisms of the in situ polyIL are separated into this "confined polymer" portion and a "bulk-like" monomer portion, suggesting that the unreacted monomer is no longer adsorbed to the silica surfaces and does not get trapped in the randomly distributed chains as would occur for the 75% polyIL/IL blend even though the chains are diluted compared to the pure bulk polymer.

The molecular picture described above is also in accordance with recent surface force apparatus measurements and simulations that describe electrostatic interactions between negatively charged flat surfaces and imidazolium NTf2-based ILs that form long-range layer formations from a few ion pairs to $\sim 1~\mu m.^{30,66-68}$ Additional evidence from surface force measurements of ILs between flat surfaces predicts that at relatively high temperatures an interplay between electrostatic interactions of silica surfaces and ions cause structural layer formations at length scales <10 nm. 28,69 These layer formations are also described as a liquid-crystalline structured phase, which would likely prefer the crystalline cis NTf2 conformations. 61 Therefore, we conclude that the electrostatic interactions associated with the silica pore walls are experienced by all ions within the pores, but the curvature of

the nanopores allows resistance to this radial layer formation. This presumption is qualitatively supported by the dielectric data that exhibit narrower $M''(\omega)$ for the *in situ* polyIL corresponding to a narrower distribution of ion dynamics times compared to the 1E3VIm NTf₂ in pores shown in Figures 2c,d and 3.

CONCLUSION

In summary, BDS and Raman spectroscopy were employed to investigate ion dynamics, coordination anion/cation pairs, and anion conformations in 1E3VIm NTf2 in bulk and under nanoscale confinement both before and after polymerization. Within the 7.5 nm diameter silica nanopores, the polymerization was found to be incomplete, resulting in ~75% conversion of the cationic monomers into polymer chains. This is attributed immobilization of monomeric cations within an adsorbed layer that results from electrostatic interactions with the pore walls. We illustrate this by showing that \sim 30% of the cations can pack into a cross-sectional pore area existing in a 0.55 surface area fraction as calculated from the ionic conductivities. Two ion dynamics processes are observed for the materials within the pores, whereas only one is observed for the same material in bulk. This suggests that separated phases are present within the pores. An increase in ionic conductivity, $\sigma'(\omega_c)$, is observed for the confined *in situ* polyIL sample compared to that in the bulk 75 wt % of a polyIL/IL blend. The Raman band at ~740 cm⁻¹ for the nanoconfined samples is shifted toward lower wavenumbers corresponding to an increase in uncoordinated anions. Additionally, the conformational equilibrium of anion conformers for the in situ polyIL is determined to be the same as that observed in the monomeric IL, while during polymerization in the bulk there is an increase in trans NTf₂ conformations at roughly 75% monomer conversion. Finally, we determined that for all of the materials measured those with higher concentrations of NTf2 C2 conformer correlate to increased ion conduction. These results are useful in a range of applications from those that require knowledge of confined dynamics of ILs and polyILs such as in batteries or supercapacitors to bioapplications such as nanochip anolyte detection and biomimetic transistors.

MATERIALS AND METHODS

The unidirectional, 50 μm thick nanoporous silica membranes with an average diameter of 7.5 \pm 1.0 nm and \sim 7% porosity were prepared by an electrochemical etching of p- $\langle 100 \rangle$, highly doped silicon wafers in an electrolyte of 1:1 volume ratio of hydrofluoric acid:ethanol as previously described. Hydrofluoric acid (HF) is corrosive and extremely toxic. Therefore, proper personal protective equipment should be worn, safety protocols followed, and training completed before and while handling HF. Anodization and electropolishing steps were performed by using 140 mA at 35 V for 40 min and 5 A at 15 V three times for 30 s each, respectively. Subsequent oxidation of the nanoporous silicon wafers was performed at 700 °C for 3 h and then at 880 °C for 6 h. 1E3VIm NTF2 (98% purity) was purchased from Iolitec and dried at 125 °C and 10^{-3} mbar for 24 h before use.

The free radical thermoinitiator, azobis(isobutyronitrile) (AIBN), was purchased from Fisher and recrystallized from methanol. The AIBN was mixed with the IL at 1.3 wt % AIBN for 24 h at room temperature while bubbling with dry N_2 for 40 min. The IL, with or without AIBN, was filled into the nanoporous silica by coating each side of the membrane with the liquid then placing it in an ultrahigh-vacuum chamber and holding it at $<10^{-8}$ mbar at room temperature for 48 h. The sample was then removed from the vacuum oven, and any excess liquid from the surface was carefully removed by wiping with KimWipes then subsequently sheared multiple times between

two clean glass slides until no detectable residual IL was transferred from the membrane surfaces to the slide. Free radical polymerization in nanopores was performed in triplicate by placing the cleaned ILfilled membrane into a Linkam THMS600 temperature stage, which was then purged for 30 min with dry N₂ before heating the material to 85 °C and holding for 24 h at the same temperature. The pure polyIL in bulk was polymerized during Raman spectroscopy with the same conditions as the in situ polyIL: solvent free with 1.3 mol % AIBN at 85 °C in the Linkam stage. This bulk polymerization was performed in triplicate, and the conversion curve (displayed as inset of Figure 1a) for each experiment was reproducible within ±1%. The resulting confined polymers' $M_{\rm n}$ were determined to be ~3 kg/mol by crushing the membranes that contained and extracting the material with d_{6} -DMSO and analyzed with end-group analysis using ¹H NMR spectroscopy (see Figure S1). The bulk polyIL was determined to have $M_n = 5.2$ kg/mol. As described in the Results and Discussion, the maximum conversion of monomeric 1E3VIm monomer to polymer was ~75% within the pores. Therefore, a bulk blend was prepared for measurement comparisons by preparing a mixture with 25 mol % monomeric 1E3VIm NTf₂ with a 3.2 kg/mol poly1E3VIm NTF₂ in tetrahydrofuran at room temperature and stirring for 12 h. The mixture was subsequently dried under vacuum at 85 °C for 48 h to remove the solvent.

Raman spectroscopy measurements were performed with a Horiba LabRAM HR Evolution Raman microscope fitted with a liquid nitrogen cooled charge coupled detector and a 648 nm excitation laser, 1800 gratings/mm, over five 2 s accumulations. A 100× objective was used for all measurements except when using the N_2 purged temperature stage for temperature-dependent measurements of solvent-free, bulk polymerization of 1E3VIm NTf₂ and subsequent temperature-dependent measurements. In this case, a long working distance (LWD) 20× objective was used. Raman measurements of the in situ polymerization under nanoconfinement were not achieved due to the small amount of IL within the pores, resulting in very low emission intensities by using the temperature stage and LWD 20× objective. Therefore, only measurements made before and after polymerization were possible. The measurement of the solvent-free, bulk polymerization was prepared by placing the 1.3 wt % AIBN/IL mixture between two glass coverslips with 0.3 mm thick Teflon spacers to maintain sample thickness and purging the temperature stage for 10 min with dry N₂. The temperature was then raised quickly to 85 °C to initiate free radical polymerization and held at 85 °C to ensure the resulting polyIL was above its $T_{\rm g}$ throughout the reaction during bulk polymerization measurements. Temperature-dependent measurements were made only after the C=C stretching mode of the vinyl monomer at 1660 cm⁻¹ had disappeared for 30 min, indicating no further detectable conversion of the C=C bond into the polymer backbone was occurring. 54,55 All Raman spectra were normalized by the intensity of the S–N–S bending mode of the NTf $_2$ anion, I_{740} , to control for changes in the density of the material during the reaction. 52,53

Dielectric experiments were performed by using a Novocontrol High Resolution Alpha dielectric analyzer with an applied ac voltage of 0.1 V over the frequency range (10^{-1} – 10^{7} Hz). Temperature was controlled with a Quatro cryostat system (180 K-400 K with a stability of ± 0.1 K). The bulk materials were sandwiched directly between two 10 mm diameter brass electrodes held at a constant thickness by sing two 200 μ m diameter glass rods. Nanopore samples were placed between two 6 mm diameter, 0.75 μ m thick aluminum foil disks to ensure sufficient electrode contact with the silica membrane and then placed between two 6 mm brass electrodes.

ASSOCIATED CONTENT

5 Supporting Information

The Supporting Information is available free of charge at https://pubs.acs.org/doi/10.1021/acsami.0c12381.

¹H NMR spectrum of *in situ* polyIL, BNN relation figure for all materials, Raman spectra over time of bulk polymerization of the monomeric IL (PDF)

AUTHOR INFORMATION

Corresponding Author

Joshua Sangoro — The Department of Chemical and Biomolecular Engineering, University of Tennessee, Knoxville, Knoxville, Tennessee 37916, United States; oocid.org/0000-0002-5483-9528; Email: jsangoro@utk.edu

Authors

- Thomas Kinsey The Department of Chemical and Biomolecular Engineering, University of Tennessee, Knoxville, Knoxville, Tennessee 37916, United States; orcid.org/0000-0002-1107-4449
- Kaitlin Glynn The Department of Chemical and Biomolecular Engineering, University of Tennessee, Knoxville, Knoxville, Tennessee 37916, United States
- Tyler Cosby Department of Chemistry, US Naval Academy, Annapolis, Maryland 21402, United States; ocid.org/ 0000-0001-6381-558X
- Ciprian Iacob National Research and Development Institute for Cryogenic and Isotopic Technologies, Valcea, Romania 240050; Karlsruhe Institute of Technology (KIT), Institute for Chemical Technology and Polymer Chemistry, Karlsruhe, Germany 76128; orcid.org/0000-0001-7982-0586

Complete contact information is available at: https://pubs.acs.org/10.1021/acsami.0c12381

Notes

The authors declare no competing financial interest.

ACKNOWLEDGMENTS

T.K., K.G., and J.S. acknowledge financial support from the National Science Foundation, the Division of Chemistry, through Grant CHE-1753282. T.C. gratefully acknowledges financial support from the U.S. Army Research Office under Contract W911NF-17-1-0052. C.I. acknowledges the financial support of the project PN 19110204 by the Romanian Ministry of Scientific Research and Innovation.

■ REFERENCES

- (1) Nakamura, K.; Saiwaki, T.; Fukao, K.; Inoue, T. Viscoelastic Behavior of the Polymerized Ionic Liquid Poly(1-ethyl-3-vinyl-imidazolium bis(trifluoromethanesulfonylimide)). *Macromolecules* **2011**, *44* (19), 7719–7726.
- (2) Li, G.; Li, Z.; Zhang, B.; Lin, Z. Developments of Electrolyte Systems for Lithium-Sulfur Batteries: A Review. *Front. Energy Res.* **2015**, 3, 1–5.
- (3) Li, M.; Yang, L.; Fang, S.; Dong, S.; Hirano, S.-i.; Tachibana, K. Polymerized Ionic Liquids with Guanidinium Cations as Host for Gel Polymer Electrolytes in Lithium Metal Batteries. *Polym. Int.* **2012**, *61* (2), 259–264.
- (4) Vicent-Luna, J. M.; Gutierrez-Sevillano, J. J.; Hamad, S.; Anta, J.; Calero, S. Role of Ionic Liquid [EMIM](+)[SCN](-) in the Adsorption and Diffusion of Gases in Metal-Organic Frameworks. ACS Appl. Mater. Interfaces 2018, 10 (35), 29694–29704.
- (5) Sangoro, J. R.; Iacob, C.; Agapov, A. L.; Wang, Y.; Berdzinski, S.; Rexhausen, H.; Strehmel, V.; Friedrich, C.; Sokolov, A. P.; Kremer, F. Decoupling of Ionic Conductivity from Structural Dynamics in Polymerized Ionic Liquids. *Soft Matter* **2014**, *10* (20), 3536–3540.
- (6) Ye, Y.; Elabd, Y. A. Anion Exchanged Polymerized Ionic Liquids: High Free Volume Single Ion Conductors. *Polymer* **2011**, *52* (5), 1309–1317.
- (7) Fan, F.; Wang, W.; Holt, A. P.; Feng, H.; Uhrig, D.; Lu, X.; Hong, T.; Wang, Y.; Kang, N.-G.; Mays, J.; Sokolov, A. P. Effect of Molecular Weight on the Ion Transport Mechanism in Polymerized Ionic Liquids. *Macromolecules* **2016**, *49* (12), 4557–4570.

- (8) Davenport, M.; Rodriguez, A.; Shea, K. J.; Siwy, Z. S. Squeezing Ionic Liquids Through Nanopores. *Nano Lett.* **2009**, 9 (5), 2125–2128.
- (9) He, Y.; Qiao, R.; Vatamanu, J.; Borodin, O.; Bedrov, D.; Huang, J.; Sumpter, B. G. Importance of Ion Packing on the Dynamics of Ionic Liquids during Micropore Charging. *J. Phys. Chem. Lett.* **2016**, 7 (1), 36–42.
- (10) Bostwick, J. E.; Zanelotti, C. J.; Iacob, C.; Korovich, A. G.; Madsen, L. A.; Colby, R. H. Ion Transport and Mechanical Properties of Non-Crystallizable Molecular Ionic Composite Electrolytes. *Macromolecules* **2020**, *53* (4), 1405–1414.
- (11) Heres, M.; Cosby, T.; Mapesa, E. U.; Liu, H.; Berdzinski, S.; Strehmel, V.; Dadmun, M.; Paddison, S. J.; Sangoro, J. Ion Transport in Glassy Polymerized Ionic Liquids: Unraveling the Impact of the Molecular Structure. *Macromolecules* **2019**, *52* (1), 88–95.
- (12) Kipnusu, W. K.; Elsayed, M.; Kossack, W.; Pawlus, S.; Adrjanowicz, K.; Tress, M.; Mapesa, E. U.; Krause-Rehberg, R.; Kaminski, K.; Kremer, F. Confinement for More Space: A Larger Free Volume and Enhanced Glassy Dynamics of 2-Ethyl-1-hexanol in Nanopores. J. Phys. Chem. Lett. 2015, 6 (18), 3708–3712.
- (13) Tu, W.; Chat, K.; Szklarz, G.; Laskowski, L.; Grzybowska, K.; Paluch, M.; Richert, R.; Adrjanowicz, K. Dynamics of Pyrrolidinium-Based Ionic Liquids under Confinement. II. The Effects of Pore Size, Inner Surface, and Cationic Alkyl Chain Length. *J. Phys. Chem. C* **2020**, *124* (9), 5395–5408.
- (14) Adrjanowicz, K.; Kaminski, K.; Tarnacka, M.; Szklarz, G.; Paluch, M. Predicting Nanoscale Dynamics of a Glass-Forming Liquid from Its Macroscopic Bulk Behavior and Vice Versa. *J. Phys. Chem. Lett.* **2017**, *8* (3), 696–702.
- (15) Tarnacka, M.; Dulski, M.; Geppert-Rybczyńska, M.; Talik, A.; Kamińska, E.; Kamiński, K.; Paluch, M. Variation in the Molecular Dynamics of DGEBA Confined within AAO Templates above and below the Glass-Transition Temperature. *J. Phys. Chem. C* **2018**, *122* (49), 28033–28044.
- (16) Kipnusu, W. K.; Elmahdy, M. M.; Elsayed, M.; Krause-Rehberg, R.; Kremer, F. Counterbalance between Surface and Confinement Effects As Studied for Amino-Terminated Poly(propylene glycol) Constraint in Silica Nanopores. *Macromolecules* **2019**, *52* (4), 1864–1873.
- (17) Lucas, R. A.; Lin, C. Y.; Baker, L. A.; Siwy, Z. S. Ionic Amplifying Circuits Inspired by Electronics and Biology. *Nat. Commun.* **2020**, *11* (1), 1568.
- (18) Vlassiouk, I.; Siwy, Z. S. Nanofluidic Diode. *Nano Lett.* **2007**, *7* (3), 552–556.
- (19) Hou, X.; Guo, W.; Jiang, L. Biomimetic Smart Nanopores and Nanochannels. *Chem. Soc. Rev.* **2011**, 40 (5), 2385–2401.
- (20) Parlak, O.; Keene, S. T.; Marais, A.; Curto, V. F.; Salleo, A. Molecularly Selective Nanoporous Membrane-based Wearable Organic Electrochemical Device for Noninvasive Cortisol Sensing. *Sci. Adv.* 2018, 4 (7), No. eaar2904.
- (21) Kim, S.; Keisham, B.; Berry, V. Cellular nano-transistor: An Electronic-interface Between Nanoscale Semiconductors and Biological Cells. *Mater. Today Nano* **2020**, *9*, 1–15.
- (22) Kanj, A. B.; Verma, R.; Liu, M.; Helfferich, J.; Wenzel, W.; Heinke, L. Bunching and Immobilization of Ionic Liquids in Nanoporous Metal-Organic Framework. *Nano Lett.* **2019**, *19* (3), 2114–2120.
- (23) Le Bideau, J.; Gaveau, P.; Bellayer, S.; Neouze, M. A.; Vioux, A. Effect of Confinement on Ionic Liquids Dynamics in Monolithic Silica Ionogels: 1H NMR study. *Phys. Chem. Chem. Phys.* **2007**, 9 (40), 5419–5422.
- (24) Garaga, M. N.; Aguilera, L.; Yaghini, N.; Matic, A.; Persson, M.; Martinelli, A. Achieving Enhanced Ionic Mobility in Nanoporous Silica by Controlled Surface Interactions. *Phys. Chem. Chem. Phys.* **2017**, *19* (8), 5727–5736.
- (25) Filippov, A.; Gnezdilov, O. I.; Hjalmarsson, N.; Antzutkin, O. N.; Glavatskih, S.; Furo, I.; Rutland, M. W. Acceleration of Diffusion in Ethylammonium Nitrate Ionic Liquid Confined Between Parallel Glass Plates. *Phys. Chem. Chem. Phys.* **2017**, *19* (38), 25853–25858.

- (26) Tripathi, A. K.; Singh, R. K. Interface and Core Relaxation Dynamics of IL Molecules in Nanopores of Ordered Mesoporous MCM-41: a Dielectric Spectroscopy study. *RSC Adv.* **2016**, *6* (51), 45147–45157.
- (27) Gebbie, M. A.; Valtiner, M.; Banquy, X.; Fox, E. T.; Henderson, W. A.; Israelachvili, J. N. Ionic liquids Behave as Dilute Electrolyte Solutions. *Proc. Natl. Acad. Sci. U. S. A.* **2013**, *110* (24), 9674–9679.
- (28) Han, M.; Espinosa-Marzal, R. M. Electroviscous Retardation of the Squeeze Out of Nanoconfined Ionic Liquids. *J. Phys. Chem. C* **2018**, *122* (37), 21344–21355.
- (29) Mezger, M.; Schroder, H.; Reichert, H.; Schramm, S.; Okasinski, J. S.; Schoder, S.; Honkimaki, V.; Deutsch, M.; Ocko, B. M.; Ralston, J.; Rohwerder, M.; Stratmann, M.; Dosch, H. Molecular Layering of Fluorinated Ionic Liquids at a Charged Sapphire (0001) Surface. *Science* **2008**, 322 (5900), 424–428.
- (30) Anaredy, R. S.; Shaw, S. K. Long-Range Ordering of Ionic Liquid Fluid Films. *Langmuir* **2016**, 32 (20), 5147–5154.
- (31) Iacob, C.; Sangoro, J. R.; Kipnusu, W. K.; Valiullin, R.; Kärger, J.; Kremer, F. Enhanced Charge Transport in Nano-confined Ionic Liquids. *Soft Matter* **2012**, *8* (2), 289–293.
- (32) Iacob, C.; Sangoro, J. R.; Papadopoulos, P.; Schubert, T.; Naumov, S.; Valiullin, R.; Karger, J.; Kremer, F. Charge Transport and Diffusion of Ionic Liquids in Nanoporous Silica Membranes. *Phys. Chem. Chem. Phys.* **2010**, *12* (41), 13798–13803.
- (33) Siwy, Z. S.; Howorka, S. Engineered Voltage-responsive Nanopores. Chem. Soc. Rev. 2010, 39 (3), 1115–1132.
- (34) Ali, M.; Mafe, S.; Ramirez, P.; Neumann, R.; Ensinger, W. Logic Gates using Nanofluidic Diodes Based on Conical Nanopores Functionalized with Polyprotic Acid Chains. *Langmuir* **2009**, *25* (20), 11993—11997.
- (35) Verma, Y. L.; Singh, R. K. Conformational States of Ionic Liquid 1-Ethyl-3-methylimidazolium Bis(trifluoromethylsulfonyl)-imide in Bulk and Confined Silica Nanopores Probed by Crystallization Kinetics Study. *J. Phys. Chem. C* **2015**, *119* (43), 24381–24392.
- (36) Nayeri, M.; Aronson, M. T.; Bernin, D.; Chmelka, B. F.; Martinelli, A. Surface Effects on the Structure and Mobility of the Ionic Liquid C6C1ImTFSI in Silica Gels. *Soft Matter* **2014**, *10* (30), 5618–5627.
- (37) Napolitano, S.; Wübbenhorst, M. The Lifetime of the Deviations from Bulk Behaviour in Polymers Confined at the Nanoscale. *Nat. Commun.* **2011**, *2* (1), 1–7.
- (38) Zhang, T.; Winey, K. I.; Riggleman, R. A. Polymer Conformations and Dynamics under Confinement with Two Length Scales. *Macromolecules* **2019**, 52 (1), 217–226.
- (39) Zhang, Q.; Archer, L. A. Effect of Surface Confinement on Chain Relaxation of Entangled cis-Polyisoprene. *Langmuir* **2003**, *19* (19), 8094–8101.
- (40) Adrjanowicz, K.; Paluch, M. Discharge of the Nanopore Confinement Effect on the Glass Transition Dynamics via Viscous Flow. *Phys. Rev. Lett.* **2019**, 122 (17), 176101.
- (41) Kinsey, T.; Mapesa, E.; Cosby, T.; He, Y.; Hong, K.; Wang, Y.; Iacob, C.; Sangoro, J. Elucidating the Impact of Extreme Nanoscale Confinement on Segmental and Chain Dynamics of Unentangled Poly(cis-1,4-isoprene). Eur. Phys. J. E: Soft Matter Biol. Phys. 2019, 42 (10) 137
- (42) Barbieri, A.; Campani, E.; Capaccioli, S.; Leporini, D. Molecular Dynamics study of the Thermal and the Density effects on the Local and the Large-scale Motion of Polymer Melts: Scaling Properties and Dielectric Relaxation. *J. Chem. Phys.* **2004**, *120* (1), 437–453.
- (43) Faria, L. F. O.; Lima, T. A.; Ribeiro, M. C. C. Phase Transitions of the Ionic Liquid [C2C1im][NTf2] under High Pressure: A Synchrotron X-ray Diffraction and Raman Microscopy Study. *Cryst. Growth Des.* **2017**, *17* (10), 5384–5392.
- (44) Pilar, K.; Baledent, V.; Zeghal, M.; Judeinstein, P.; Jeong, S.; Passerini, S.; Greenbaum, S. Communication: Investigation of Ion Aggregation in Ionic Liquids and Their Solutions with Lithium Salt under High Pressure. *J. Chem. Phys.* **2018**, *148* (3), 031102.

- (45) Talik, A.; Tarnacka, M.; Dzienia, A.; Kaminska, E.; Kaminski, K.; Paluch, M. High-Pressure Studies on the Chain and Segmental Dynamics of a Series of Poly(propylene glycol) Derivatives. *Macromolecules* **2019**, 52 (15), 5658–5669.
- (46) Wojnarowska, Z.; Knapik, J.; Jacquemin, J.; Berdzinski, S.; Strehmel, V.; Sangoro, J. R.; Paluch, M. Effect of Pressure on Decoupling of Ionic Conductivity from Segmental Dynamics in Polymerized Ionic Liquids. *Macromolecules* **2015**, *48* (23), 8660–
- (47) Maksym, P.; Tarnacka, M.; Dzienia, A.; Erfurt, K.; Chrobok, A.; Zięba, A.; Wolnica, K.; Kaminski, K.; Paluch, M. A Facile Route to Well-defined Imidazolium-based Poly(ionic liquid)s of Enhanced Conductivity via RAFT. *Polym. Chem.* **2017**, 8 (35), 5433–5443.
- (48) Tarnacka, M.; Chrobok, A.; Matuszek, K.; Golba, S.; Maksym, P.; Kaminski, K.; Paluch, M. Polymerization of Monomeric Ionic Liquid Confined within Uniaxial Alumina Pores as a New Way of Obtaining Materials with Enhanced Conductivity. ACS Appl. Mater. Interfaces 2016, 8 (43), 29779–29790.
- (49) Yu, Z.; Fang, C.; Huang, J.; Sumpter, B. G.; Qiao, R. Molecular Structure and Dynamics of Interfacial Polymerized Ionic Liquids. *J. Phys. Chem. C* **2018**, *122* (39), 22494–22503.
- (50) Ganesan, V. Ion Transport in Polymeric Ionic Liquids: Recent Developments and Open Ouestions. *Molecular Systems Design & Engineering* **2019**, *4* (2), 280–293.
- (51) Heres, M.; Cosby, T.; Mapesa, E. U.; Sangoro, J. Probing Nanoscale Ion Dynamics in Ultrathin Films of Polymerized Ionic Liquids by Broadband Dielectric Spectroscopy. *ACS Macro Lett.* **2016**, 5 (9), 1065–1069.
- (52) Paschoal, V. H.; Faria, L. F. O.; Ribeiro, M. C. C. Vibrational Spectroscopy of Ionic Liquids. *Chem. Rev.* **2017**, *117* (10), 7053–7112.
- (53) Xuan, X.; Guo, M.; Pei, Y.; Zheng, Y. Theoretical Study on Cation-Anion Interaction and Vibrational Spectra of 1-allyl-3-methylimidazolium-based Ionic Liquids. *Spectrochim. Acta, Part A* **2011**, 78 (5), 1492–1499.
- (54) Minamimoto, H.; Irie, H.; Uematsu, T.; Tsuda, T.; Imanishi, A.; Seki, S.; Kuwabata, S. Polymerization of Room-temperature Ionic Liquid Monomers by Electron Beam Irradiation with the aim of Fabricating Three-dimensional Micropolymer/Nanopolymer Structures. *Langmuir* **2015**, *31* (14), 4281–4289.
- (55) Giussi, J. M.; Blaszczyk-Lezak, I.; Cortizo, M. S.; Mijangos, C. In-situ Polymerization of Styrene in AAO Nanocavities. *Polymer* **2013**, 54 (26), 6886–6893.
- (56) Mogurampelly, S.; Ganesan, V. Ion Transport in Polymerized Ionic Liquid–Ionic Liquid Blends. *Macromolecules* **2018**, *51* (23), 9471–9483.
- (57) Holbrey, J. D.; Reichert, W. M.; Rogers, R. D. Crystal Structures of imidazolium bis(trifluoromethanesulfonyl)imide 'Ionic Liquid' Salts: The First Organic Salt with a cis-TFSI Anion Conformation. *Dalton Trans* **2004**, No. 15, 2267–2271.
- (58) Lassègues, J. C.; Grondin, J.; Holomb, R.; Johansson, P. Raman and ab initio study of the Conformational Isomerism in the 1-ethyl-3-methyl-imidazolium bis(trifluoromethanesulfonyl)imide Ionic Liquid. *J. Raman Spectrosc.* **2007**, 38 (5), 551–558.
- (59) Lopes, J. N.; Shimizu, K.; Padua, A. A.; Umebayashi, Y.; Fukuda, S.; Fujii, K.; Ishiguro, S. A Tale of Two Ions: the Conformational Landscapes of bis(trifluoromethanesulfonyl)amide and N, N-dialkylpyrrolidinium. *J. Phys. Chem. B* **2008**, *112* (5), 1465–1472.
- (60) Fujii, K.; Fujimori, T.; Takamuku, T.; Kanzaki, R.; Umebayashi, Y.; Ishiguro, S. Conformational Equilibrium of bis-(trifluoromethanesulfonyl) imide Anion of a Room-temperature Ionic Liquid: Raman Spectroscopic study and DFT calculations. *J. Phys. Chem. B* **2006**, *110* (16), 8179–8183.
- (61) Forsyth, C. M.; MacFarlane, D. R.; Golding, J. J.; Huang, J.; Sun, J.; Forsyth, M. Structural Characterization of Novel Ionic Materials Incorporating the Bis(trifluoromethanesulfonyl)amide Anion. *Chem. Mater.* **2002**, *14* (5), 2103–2108.

- (62) Kiefer, J.; Fries, J.; Leipertz, A. Experimental Vibrational Study of Imidazolium-based Ionic Liquids: Raman and Infrared spectra of 1-ethyl-3-methylimidazolium bis(trifluoromethylsulfonyl)imide and 1-ethyl-3-methylimidazolium ethylsulfate. *Appl. Spectrosc.* **2007**, *61* (12), 1306–1311.
- (63) Duluard, S.; Grondin, J.; Bruneel, J.-L.; Pianet, I.; Grélard, A.; Campet, G.; Delville, M.-H.; Lassègues, J.-C. Lithium Solvation and Diffusion in the 1-butyl-3-methylimidazolium bis-(trifluoromethanesulfonyl)imide Ionic Liquid. *J. Raman Spectrosc.* 2008, 39 (5), 627–632.
- (64) Patel, H. K.; Martin, S. W. Fast Ionic Conduction inNa2S +B2S3glasses: Compositional Contributions to Nonexponentiality in Conductivity Relaxation in the Extreme Low-alkali-metal Limit. *Phys. Rev. B: Condens. Matter Mater. Phys.* **1992**, 45 (18), 10292–10300.
- (65) Iacob, C.; Runt, J. Charge Transport of Polyester Ether Ionomers in Unidirectional Silica Nanopores. *ACS Macro Lett.* **2016**, 5 (4), 476–480.
- (66) Ori, G.; Villemot, F.; Viau, L.; Vioux, A.; Coasne, B. Ionic Liquid Confined in Silica Nanopores: Molecular Dynamics in the Isobaric—isothermal Ensemble. *Mol. Phys.* **2014**, *112* (9–10), 1350–1361
- (67) Wakeham, D.; Hayes, R.; Warr, G. G.; Atkin, R. Influence of Temperature and Molecular Structure on Ionic Liquid Solvation Layers. J. Phys. Chem. B 2009, 113 (17), 5961–5966.
- (68) Garcia, L.; Jacquot, L.; Charlaix, E.; Cross, B. Nano-mechanics of Ionic Liquids at Dielectric and Metallic Interfaces. *Faraday Discuss.* **2018**, *206*, 443–457.
- (69) Gebbie, M. A.; Smith, A. M.; Dobbs, H. A.; Lee, A. A.; Warr, G. G.; Banquy, X.; Valtiner, M.; Rutland, M. W.; Israelachvili, J. N.; Perkin, S.; Atkin, R. Long Range Electrostatic forces in Ionic Liquids. *Chem. Commun.* (*Cambridge, U. K.*) **2017**, 53 (7), 1214–1224.
- (70) Sailor, M. J. Porous Silicon in Practice; Wiley-VCH Verlag & Co.: Weilheim, Germany, 2011.

Supporting Information:

Ion dynamics of Monomeric Ionic Liquids Polymerized *in situ* within Silica Nanopores

Thomas Kinsey¹, Kaitlin Glynn¹, Tyler Cosby², Ciprian Iacob^{3,4}, and Joshua Sangoro*¹

- ¹⁾ The Department of Chemical and Biomolecular Engineering, University of Tennessee, Knoxville, Knoxville, TN 37916
- ²⁾ Department of Chemistry, US Naval Academy, Annapolis, MD 21402
- ³⁾ National Research and Development Institute for Cryogenic and Isotopic Technologies, ICSI Rm. Valcea, Romania 240050
- ⁴⁾ Karlsruhe Institute of Technology (KIT), Department for Chemical Technology and Polymer Chemistry, Karlsruhe, Germany 76128
- *Corresponding Author Email: jsangoro@utk.edu

Figure S1 is the 1 H NMR spectrum of the *in-situ* polyIL. After *in-situ* polymerization within the nanopores, and subsequent dielectric and Raman spectroscopy measurements, the polyIL-filled membranes were ground into a fine powder. This powder, containing broken nanoporous silica, polyIL and unreacted IL monomer, was then added to roughly 1.5 mL of d_6 -DMSO to dissolve the organic IL and polyIL. This sample was then measured by 1 H NMR. The peaks in Figure S1 match the corresponding hydrogen nuclei that are labeled in the schematic of the monomeric cation and cationic repeat unit. The peak labeled "h" corresponds to the six hydrogens in the polymer end group that come from the AIBN initiator. The relative values of peak integration (x_i) are displayed below the peaks themselves. These integral values are divided by the number of hydrogens they represent when calculating relative amounts of each molecule. This concludes a relative fraction of un-converted monomer to be 0.3 which compares well with the polymer fraction as determined by Raman Spectroscopy. By end group analysis, the *in-situ* polymer molecular weight is \sim 3 kg/mol.

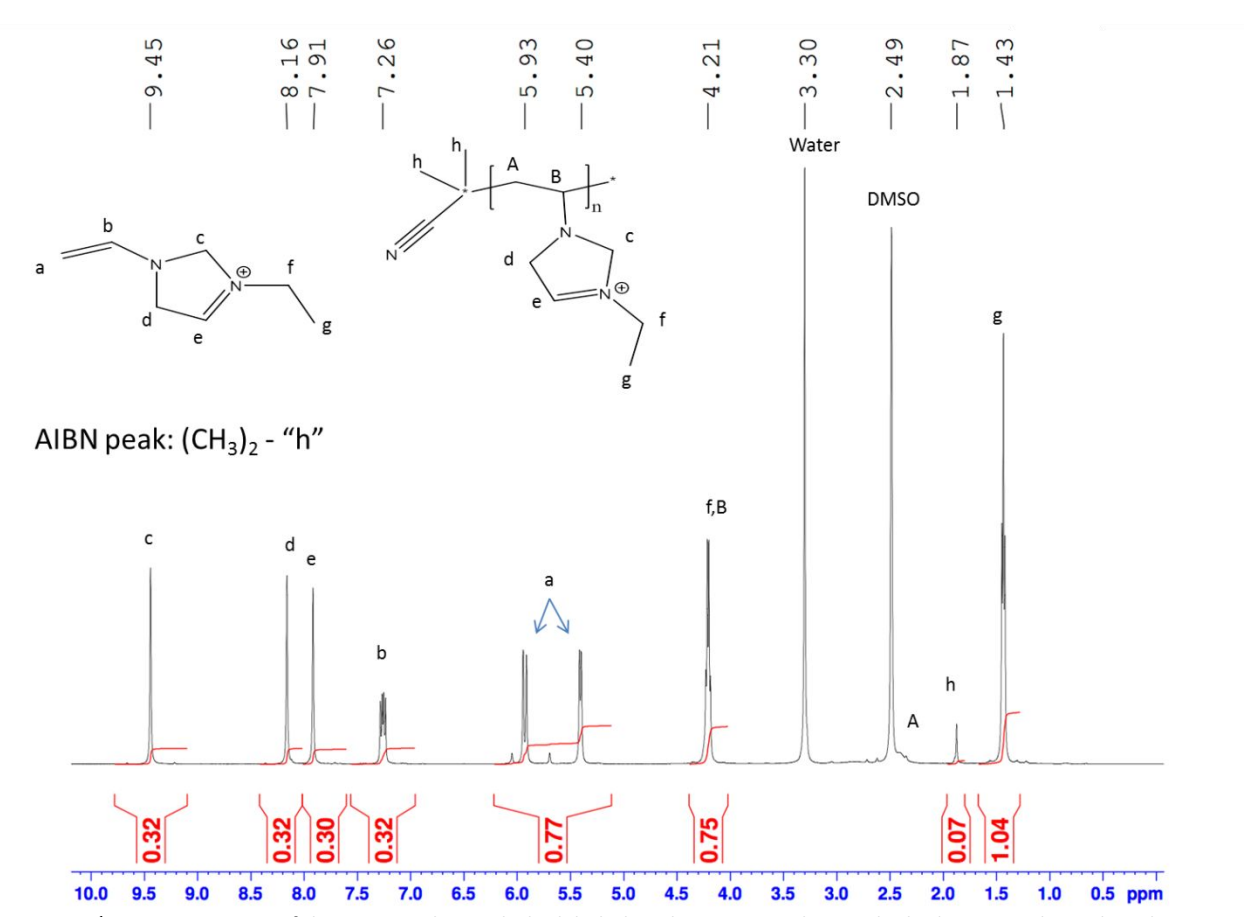


Figure S1: ¹H NMR spectrum of the *in-situ* polyIL with the labeled peaks corresponding to the hydrogen nuclei in the schematic monomeric cation, cationic repeat unit, and polyIL end group.

Figure S2 below is the log-log plot of the real part of conductivity value at the characteristic ion hopping rate vs the characteristic ion hopping rate for all samples except the monomer in bulk. The *in-situ* polyIL and 1E3VIm NTf₂ in pores are provided here for all of the triplicate samples. The bulk polymer, bulk 75% polyIL/IL blend, and bulk-like conductivities for the monomer and polymerized samples in pores are shown as stars, crossed diamonds, and solid and open circles, respectively (with a solid line for a guide). All of these data fall on the same line and correlate with the BNN relation of the random barrier model of AC to DC ion conduction¹. The "confined" monomer and polymer conductivities, as shown in Figure 4 of the main text, are observed to have an increased value of conductivity for the corresponding ion hopping rate as observed in the closed and open circles (with a dashed line as a guide).

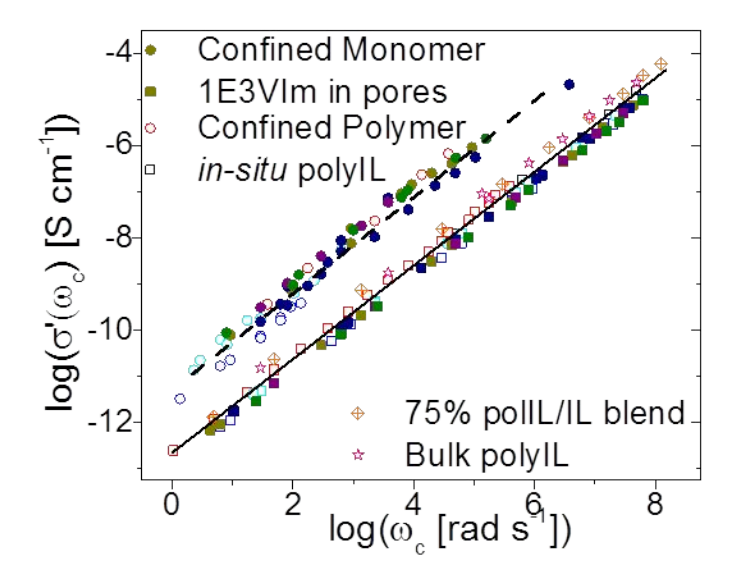


Figure S2: BNN plot for all triplicate samples in pores for the monomer and polymerized sample, and also for the polymer containing materials in bulk. The corresponding log conductivity vs 1000/T data are found in Figure 4 of the main text.

Figure S3 (top) is the temperature dependent bulk polyIL Raman peaks for the *cis/trans* conformational isomer of the NTf₂ anion. The ratio of these two peaks are used to calculate the equilibrium conformational enthalpy change from *cis* to *trans* ($\Delta H_{conf} = 2.45 \text{ kJ/mol}$) with increasing temperature for these two isomers as shown in the inset. This enthalpy changes is slightly decreased compared to the value for a similar monomeric ionic liquid in bulk from the literature (1-ethyl-3-methylimidazolium NTf₂, $\Delta H_{conf} = 3.5 \text{ kJ/mol}$)². Additionally, with increasing temperature the S-N-S bending mode of the anion shifts toward higher wavenumbers and is shown in Figure S3(bottom). This shift corresponds to an increase in free NTf₂ with increasing temperature.

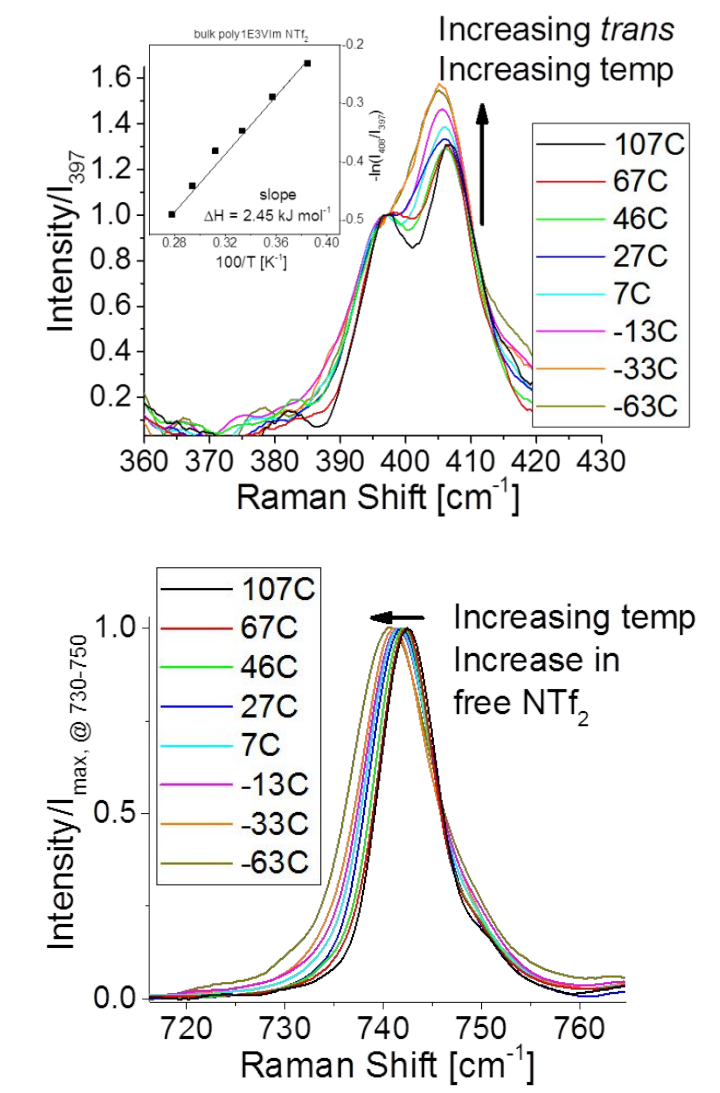


Figure S3: Temperature dependent Raman

spectrum for the NTf₂ vibrational modes of the *cis-trans* isomers (top) and S-N-S bending mode (bottom).

REFERENCES

- 1. Dyre, J. C., The random free-energy barrier model for ac conduction in disordered solids. *Journal of Applied Physics* **1988**, *64* (5), 2456-2468.
- 2. Fujii, K.; Fujimori, T.; Takamuku, T.; Kanzaki, R.; Umebayashi, Y.; Ishiguro, S., Conformational equilibrium of bis(trifluoromethanesulfonyl) imide anion of a room-temperature ionic liquid: Raman spectroscopic study and DFT calculations. *J Phys Chem B* **2006**, *110* (16), 8179-83. 8179-8183.